Recent Results from Edge Modellingon ASDEX Upgrade

D.P. Coster[a], X. Bonnin[b], A.V. Chankin[a], H.-J. Klingshirn[a], C. Konz[a], G. Pautasso[a], M. Wischmeier[a], E. Wolfrum[a] and the ASDEX Upgrade Team

[a]Max-Planck-Institut für Plasmaphysik, EURATOM Association, D-85748 Garching, Germany.
[b] CNRS-LIMHP, Université Paris 13, F-93430 Villetaneuse, France

e-mail: David.Coster@ipp.mpg.de

Abstract Recent results obtained from modelling the edge plasma of ASDEX Upgrade (AUG) are presented, including detailed simulations of a few discharges where upstream and target data from the experiment were compared with the code results, detailed simulations of a series of discharges targeted at understanding the processes of divertor detachment, simulations of a discharge where a transition from L-mode to H-mode was triggered solely by a drop in the toroidal magnetic field, simulations of the penetration of Massive Gas Injection (MGI) gas puffs used for disruption mitigation, simulations to examine the effect of ELM "size" on the whole plasma and simulations of Tungsten.

1. Introduction

The modelling used the SOLPS suite of codes [1–3] (and references therein) to simulate the divertor, Scrape-Off Layer (SOL) and either a part of or the whole main plasma. The main component of the suite consists of the combination of a 2D fluid plasma transport code (B2.5) and a 3D Monte-Carlo neutrals transport code (Eirene), although, for some of the work, a neutral fluid model was used in place of the more accurate kinetic model.

In order to perform the work described below, modifications have been made over the last few years to the standard SOLPS code package. The relevant modifications are described in the relevant physics sections below.

In this paper we cover recent results obtained from modelling the edge plasma of ASDEX Upgrade (AUG): detailed simulations of a few discharges where upstream and target data from the experiment were compared with the code results (section 2); detailed simulations of a series of AUG discharges targeted at understanding the processes of divertor detachment (section 3); the simulation of a discharge where a transition from L-mode to H-mode was triggered solely by a drop in the toroidal magnetic field (section 4); simulations of the penetration of Massive Gas Injection (MGI) gas puffs used for disruption mitigation (section 5); simulations to examine the effect of ELM "size" on the whole plasma (section 6); simulations of Tungsten (section 7). The paper concludes with a discussion and some plans for the further development of the code (section 8).

2. Detailed modelling of a limited number of shots

AUG is ideally suited for improving our understanding of the edge plasma because of excellent diagnostic coverage of both the upstream and target plasmas. Knowledge of the heating power, radiated power, gas puff and pumped flux, together with excellent upstream profiles of n_e, T_e and T_i are used to constrain the "free" parameters of the simulation — i.e. to determine profiles of D, χ_e and χ_i, as well as the boundary conditions. The resultant "predictions" of the target quantities are then compared to those experimentally measured. When this was done for an H-mode discharge, discrepancies were

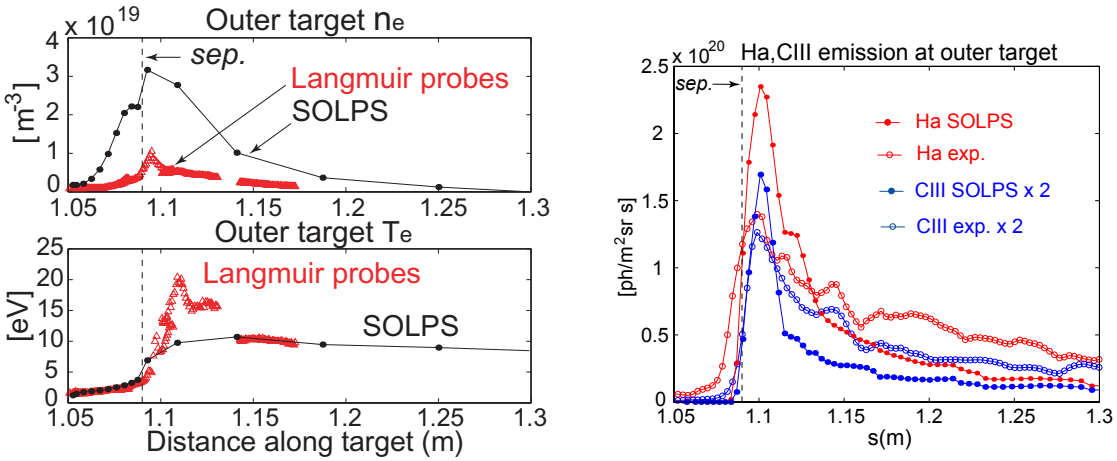

Figure 1: Discrepancy between detailed code modelling and the experimental results. Left from [4], right from [5].

found in that the code tended to predict a denser, colder plasma at the target than that measured (resulting in, for example, a factor two difference in the H_α radiation). At the same time, the measured upstream E_r was higher than that predicted by the code, and the measured parallel flows upstream higher than those predicted by the code. (Similar results have been seen on other tokamaks and with other edge codes.) Despite a large variation in the "free" parameters, the discrepancy between the experiment and code could not be eliminated (see for example figure 1). A possible explanation for the divertor density over-estimate and divertor temperature under-estimate is the presence of kinetic effects in this region not present in the fluid plasma description. When parameters are varied so as to produce a hotter divertor plasma (e.g. by dropping the upstream density below that measured experimentally), the E_r from the code is found to approach that measured experimentally, and the parallel flows are also found to approach the experimental ones. Results of these simulations are shown in [6] (and references therein).

The comparison with experimental results was aided by the use of the MDSplus interface to the SOLPS results [7] which allows for the easy comparison of code and experimental results.

3. Modelling of detachment

Since the ITER divertor design currently relies on partial divertor detachment to lower the energy fluxes to the targets, it is important to investigate the ability of the edge codes to properly capture this physics. A series of well diagnosed Ohmic discharges were performed on AUG with increasing flat-top density against which numerical simulations are compared [8]. Whilst the code reproduces qualitatively the behaviour of the peak ion flux densities, Γ_i, at the outer target, the experimentally observed continuous decrease of Γ_i as a function of the flat-top density is not reproduced. However, changes in the model of the conductances below the dome and divertor target plates lead to a non-increasing Γ_i at the inner target and absolute values of Γ_i at the outer target that are within a factor of 1.5 of the experimental data.

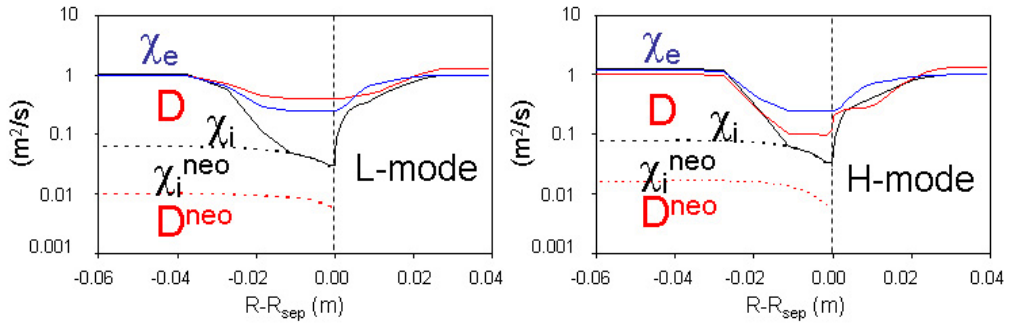

Figure 2: Derived transport coefficients.

4. Modelling of L- and H-mode discharges

The nature of the L-mode to H-mode transition remains a challenge. In order to better characterize some of the differences between these two regimes, a transition was triggered in an AUG discharge by lowering the magnetic field while keeping the heating power and density as constant as possible. Detailed modelling of these two phases showed that the electron and ion heat transport coefficients required to match the upstream profiles hardly changed (and that the ion heat transport was close to neo-classical values even in the L-mode), but that the particle diffusivity changed significantly, see figure 2. (For additional information, see Wolfrum *et al*, this conference.)

For these simulations the neo-classical contributions to the transport coefficients were included [9]. This work is based on the neoclassical model of Hirshman and Sigmar [10] and Peeters and its numerical implementation [11]. The diffusive and convective contributions to the neo-classical particle and heat fluxes

$$\begin{aligned} \Gamma_{aj} &= -D_{aj}\nabla n_{aj} + v_{aj} n_{aj} \\ q_{aj} &= -\kappa_{aj}\nabla T_a + w_{aj} T_a \end{aligned} \tag{1}$$

are calculated for given thermodynamic forces

$$F^{\mathrm{p}}_{aj} = \frac{\partial \ln p_{aj}}{\partial \rho}$$

$$F^{\mathrm{T}}_{aj} = \frac{\partial \ln T_a}{\partial \rho} \tag{2}$$

$$(\rho = \text{flux label},\ a = \text{species},\ j = \text{charge state}) \tag{3}$$

and external electric field E and added to the classical and anomalous fluxes. The model calculates both Banana-Plateau and Pfirsch-Schlüter contributions to the neo-classical transport and is therefore suited for application in the plasma core and edge regions with exception of steep gradient regions where the validity of the neo-classical formulation has to be tested for each ion species.

The transport model is one dimensional and therefore limited to closed flux surfaces. A matching of the neo-classical 1D core transport to the fluid drift modelling of 2D transport in the SOL is foreseen as a further expansion of the B2 fluid model.

5. Modelling of Massive Gas Injection

Massive Gas Injection (MGI) gas puffs have been suggested as a tool to mitigate disruptions and to suppress run-away electron production. The simulation of the penetration of

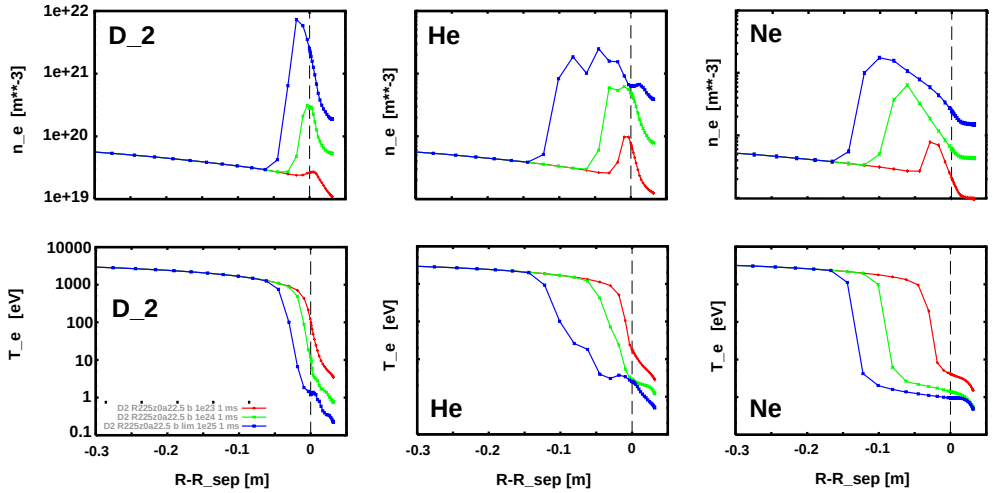

Figure 3: Results of simulations for D_2, He and Ne gas puffs with puff rates of 1×10^{23} (red), 1×10^{24} (green) and 1×10^{25} (blue) particles per second, all taken at $1ms$ after the start of the gas-puff.

the neutrals into the plasma presents a number of challenges: (1) the experimental situation tends to be 3D while the readily available tools are 2D; (2) the large influx of neutrals changes the plasma conditions on a very fast time-scale and in a way that is a challenge to the numerics of the codes; (3) additional physics (such as global/large scale MHD modes, field reconnection and increased turbulence) outside that in the transport codes is also likely to play a role. With these *caveats* in mind, an effort has been started to simulate the effects of very large gas puffs (10^{23} – 10^{25} particles/sec for a few milliseconds) using D_2, He and Ne, and to compare the code results with those from the experiment [12]. To capture some of the additional effects, simulations with changed transport coefficients were also performed, (see Pautasso *et al.*, this conference).

When neutral sources are present, the energy content carried by the ionized neutrals must be converted into kinetic (directed) and thermal (undirected) energy delivered to the ions. The former term also imparts momentum to the ion fluid, while the latter term modifies the ion temperature. Basically, we apply the following conversion rules, where the E superscript represents the energy sources in Eirene and H the heat sources in B2.5:

$$\text{total energy} \Rightarrow \quad S_a^E = \int \frac{1}{2} m_a v_a^2 S_a^{particle} \, d^3\vec{v}, \tag{4}$$

$$\text{internal energy} \Rightarrow \quad S_a^H = \int \frac{1}{2} m_a \left(\vec{v}_a - \vec{u}_a\right)^2 S_a^{particle} \, d^3\vec{v}, \tag{5}$$

$$\rightarrow \quad S_a^H = S_a^E - \vec{u}_a \cdot \vec{S}_a^{mom} + \frac{1}{2} m_a u_a^2 S_a^{particle}. \tag{6}$$

However, Eq.(6) implicitly assumes that the perturbation caused by the neutrals on the ion fluid is small and is, in that sense, a "first-order" correction. Specifically, it requires that the plasma species density n_a and parallel velocity u_a change slowly on the timescale of the timestep Δt. In the case of MGI gas puffs, this is no longer the case, and Eq.(6) needs to be generalized as detailed below. Including all terms, the ion heat source over a

timestep is given by:

$$S_i^H \Delta t = \sum_a \left(n_a^t + S_a^{particle}\Delta t\right) \left\langle \frac{1}{2} m_a (\vec{v}_a - \vec{u}_a)^2 \right\rangle^{t+\Delta t} - \sum_a n_a^t \left\langle \frac{1}{2} m_a (\vec{v}_a - \vec{u}_a)^2 \right\rangle^{t} \quad (7)$$

with

$$\vec{u}_a^{t+\Delta t} = \langle \vec{v}_a \rangle^{t+\Delta t} = \frac{n_a^t \vec{u}_a^t + \frac{1}{m_a}\vec{S}_a^{mom}\Delta t}{n_a^t + S_a^{particle}\Delta t}$$

$$\delta \vec{u}_a = \vec{u}_a^{t+\Delta t} - \vec{u}_a^t = \frac{\frac{1}{m_a}\vec{S}_a^{mom}\Delta t - \vec{u}_a^t S_a^{particle}\Delta t}{n_a^t + S_a^{particle}\Delta t}$$

and the brackets $\langle \cdots \rangle$ denote an average over the ion distribution function. A little algebra yields:

$$\left\langle \frac{1}{2} m_a (\vec{v}_a - \vec{u}_a)^2 \right\rangle^{t+\Delta t} = \left\langle \frac{1}{2} m_a \left(\vec{v}_a - \vec{u}_a^t\right)^2 \right\rangle^{t+\Delta t} - \frac{1}{2} m_a (\delta \vec{u}_a)^2$$

Writing the first term of the R.H.S. explicitly:

$$\left\langle \frac{1}{2} m_a \left(\vec{v}_a - \vec{u}_a^t\right)^2 \right\rangle^{t+\Delta t} = \frac{1}{n_a^t + S_a^{particle}\Delta t} \times \left[\frac{3}{2} n_a^t T_a^t + S_a^E \Delta t + \frac{1}{2} m_a {u_a^t}^2 S_a^{particle}\Delta t - \vec{u}_a^t \cdot \vec{S}_a^{mom}\Delta t\right]$$

Putting all this back into Eq. (7), we obtain:

$$\begin{aligned} S_i^H \Delta t = & \\ & \sum_a \left[\frac{3}{2} n_a^t T_a^t + S_a^E \Delta t + \frac{1}{2} m_a {u_a^t}^2 S_a^{particle}\Delta t - \vec{u}_a^t \cdot \vec{S}_a^{mom}\Delta t\right] - \\ & \sum_a \left[\left(n_a^t + S_a^{particle}\Delta t\right) \frac{1}{2} m_a (\delta u_a)^2\right] - \\ & \sum_a \frac{3}{2} n_a^t T_a^t \end{aligned}$$

Thus:

$$S_i^H = \sum_a S_a^E - \sum_a \vec{u}_a^t \cdot \vec{S}_a^{mom} + \sum_a \frac{1}{2} m_a {u_a^t}^2 S_a^{particle} - \sum_a \frac{n_a^t + S_a^{particle}\Delta t}{\Delta t} \frac{1}{2} m_a (\delta u_a)^2 \quad (8)$$

In the code, we previously had only the first three terms in the R.H.S. of the final equation (8) above. But for very strong sources, dominating the background plasma, the higher order correction is necessary. Without these changes, at the higher particle puff rates, instead of a cooling of the plasma, a temperature rise was seen.

6. Modelling of the effects of ELMS on the core and edge plasma

When exploring edge-core effects in simulations, three approaches have been used: *direct* coupling where a 2D edge code is coupled at a surface (usually the separatrix) to the 1D

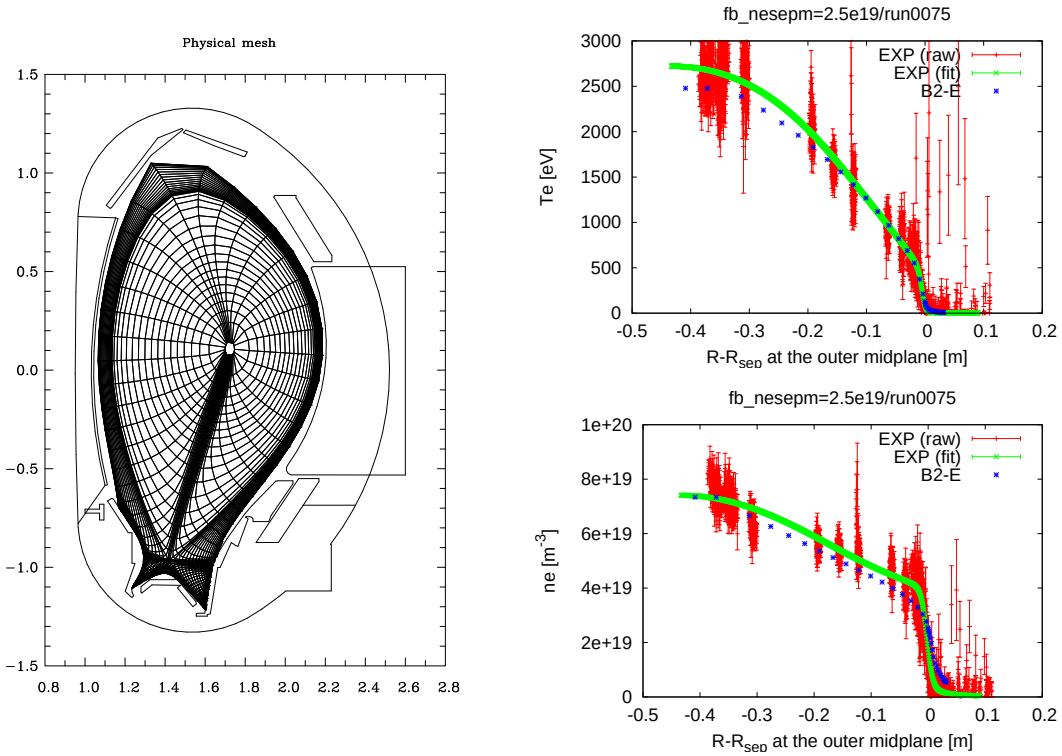

Figure 4: Geometry used (left panel) and experimental and fitted profiles (right panel) of electron temperature (top) and electron density (bottom) along the outer midplane from experiment and the code.

core code; *mediated* coupling where the 2D results are parameterized in some form and are then used to provide better boundary conditions for the 1D core code; and *avoided* where the 2D edge code is used over the whole domain. This third approach has been used to look at the effects of ELM size on the whole plasma for AUG simulations. To do this, a set of radial anomalous transport coefficients and sources (particles and heating) were taken from a 1D simulation of a particular AUG discharge, and then used for a series of simulations where: (1) the effect of ELM "size" (depth of region directly affected by the ELM, transport enhancement factor during the ELM event) on both the core and edge was investigated; (2) the main plasma density of the ELMing plasma was varied under feedback control of an edge gas-puff; (3) the effect of the heat pulses on the target was investigated using a thermal model for the plates.

The geometry used, and the midplane electron temperature and density from the experiment and one of the simulations are shown in figure 4. Some results have been presented in [13]. For these simulations, some modifications of the code were necessary to ensure zero flux boundary conditions at the core boundary by implementing a feedback control of the core density.

7. Modelling of Tungsten

Following work by Pütterich *et al.* and the ADAS group [14] on tungsten atomic data and bundling of charge states, it is now possible to simulate realistically AUG in its new full-W wall configuration. Currently, SOLPS runs are ongoing with a detailed wall model

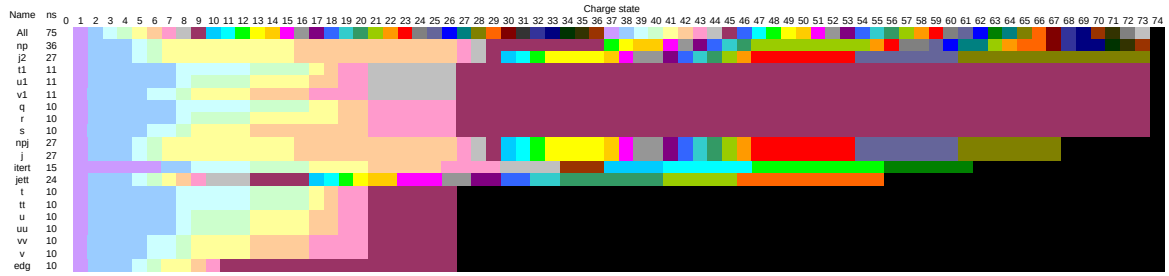

Figure 5: Different W bundles used.

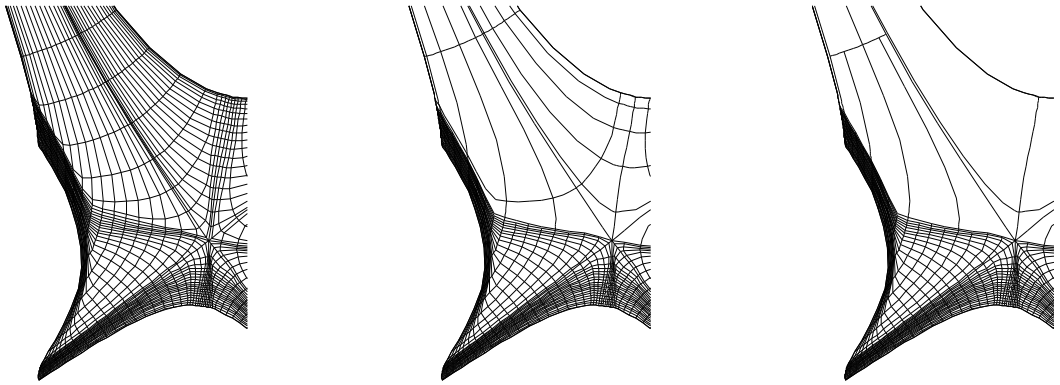

Figure 6: Differing levels of mesh refinement.

tracking erosion and redeposition of wall material. The goal of these runs is to compare the impact of various bundling schemes (with varying emphasis on charge states being bundled and aggressiveness in the reduction of the number of W species in the simulations, down to 9 bundles for the most aggressive, see figure 5) on the full edge plasma solution, and also comparing to runs with the full complement of W charge states.

This work builds on changes [15–17] to the B2 part of SOLPS5 that incorporate a detailed wall model, including a thermal model for the target plates, enhanced erosion processes, an erosion/deposition/re-erosion model and, most recently, the incorporation of the ability to bundle different charge states together so as to reduce the computational demands.

8. Discussion and planned updates to the code

There is always a balancing act between the use of a code such as SOLPS *versus* the further development of the code. In the above sections, physics results have been bracketed with the code updates required to produce those results. Other work on the code is longer term, such as the better treatment of "drift" terms and the improvement of the basic "numerics". This second aspect is discussed briefly below.

Work has continued on extending the B2 code to support grid adaptation. The basis for this approach is to recast the solver to work on fully unstructured grids. These working grids consist of logically rectangular control volumes and are built by joining control volumes starting from a finest possible field-aligned base grid as supplied by the grid generator. Algorithms have been developed that support both isotropic and anisotropic grid refinement and coarsening of the unstructured working grids. The adaptation mechanism supports configurable strategies to expand local adaptation requests as required to make the resulting grids comply to the restrictions given by the grid data structure.

An example is given in figure 6 for a typical B2 grid, where, starting from the finest possible grid, the grid resolution is kept fixed in the divertor region, and is coarsened in the rest of the domain. At the same time, the finite volume discretization in the core solver for the fluid equations is being redesigned to match the changed requirements of the unstructured grid. Emphasis is put on efficiency in order to offset the performance penalty introduced by having to handle a more complex grid connectivity.

References

[1] COSTER, D. et al., Recent developments in tokamak edge physics analysis at Garching, in *Proc. of the 18th IAEA Conference, Fusion Energy, Sorrento, Italy, October 2000, (CD-ROM)*, pages IAEA–CN–77/EXP5/32, Vienna, 2000, IAEA.

[2] COSTER, D. et al., Further developments of the edge transport simulation package, SOLPS, in *Proc. of the 19th IAEA Conference, Fusion Energy, Lyon, France, October 2002, (CD-ROM)*, pages IAEA–CN–94/TH/P2–13, Vienna, 2002, IAEA.

[3] SCHNEIDER, R. et al., Contrib. Plasma Phys. **46** (2006) 3, DOI 10.1002/ctpp.200610001.

[4] CHANKIN, A. V. et al., J. Nucl. Mater. **363–365** (2007) 335.

[5] CHANKIN, A. V. et al., Plasma Phys. Controlled Fusion **48** (2006) 839.

[6] CHANKIN, A. V. et al., Nucl. Fusion **47** (2007) 762.

[7] COSTER, D. P., Time dependent SOL modelling with SOLPS, in *Europhysics Conference Abstracts (CD-ROM, Proc. of the 30th EPS Conference on Controlled Fusion and Plasma Physics, St. Petersburg, 2003)*, edited by KOCH, R. et al., volume 27A, pages P–1.169, Geneva, 2003, EPS.

[8] WISCHMEIER, M. et al., Contrib. Plasma Phys. **48** (2008) 249, DOI 10.1002/ctpp.200810043.

[9] KONZ, C. et al., Neoclassical transport in the plasma edge at ASDEX Upgrade with B2, in *Europhysics Conference Abstracts (CD-ROM, Proc. of the 31st EPS Conference on Plasma Physics, London, 2004)*, edited by NORREYS, P. et al., volume 28G, pages P–4.122, Geneva, 2004, EPS.

[10] HIRSHMAN, S. P. et al., Nucl. Fusion **21** (1981) 1079.

[11] PEETERS, A. G., Plasma Phys. Controlled Fusion **42** (2000) B231.

[12] PAUTASSO, G. et al., Modelling of massive gas injection with solps, in *Europhysics Conference Abstracts (CD-ROM, Proc. of the 35th EPS Conference on Plasma Physics, Crete, 2008)*, Geneva, 2008, EPS.

[13] COSTER, D., Whole device ELM simulations, presented at the 2008 Plasma Surface Interactions Conference and submitted to Journal of Nuclear Materials.

[14] PÜTTERICH, T. et al., Plasma Phys. Controlled Fusion **50** (2008) 085016.

[15] COSTER, D. et al., Integrated modelling of material migration and target plate power handling at JET, in *Proc. of the 20th IAEA Conference Fusion Energy (CD-Rom), Vilamoura, Portugal, November 2004*, volume 0, pages IAEA–CN–116/TH/P5–18, Vienna, 2005, IAEA.

[16] COSTER, D. P. et al., J. Nucl. Mater. **363–365** (2007) 136.

[17] BONNIN, X. et al., Integrated modelling of plasma-wall interactions in tokamaks with B2.5: mixed materials, layers and coatings, bundled charge states, and hydrogen inventory, in *Europhysics Conference Abstracts (CD-ROM, Proc. of the 34th EPS Conference on Plasma Physics, Warsaw, 2007)*, Geneva, 2007, EPS.